Chinese Chemical Letters 34 (2023) 107664

Contents lists available at ScienceDirect

Chinese Chemical Letters

journal homepage: www.elsevier.com/locate/cclet

Facile preparation of α-MnO_2 nanowires for assembling free-standing membrane with efficient Fenton-like catalytic activity

Yufei Zhen[a], Zhiqiang Sun[a,*], Ziye Jia[a], Caihong Liu[b], Shishu Zhu[c,d,**], Xueyan Li[e], Wei Wang[a], Jun Ma[a]

[a] School of Environment, State Key Laboratory of Urban Water Resources and Environment, Harbin Institute of Technology, Harbin 150090, China
[b] Key Laboratory of Eco-Environments in Three Gorges Reservoir Region, Ministry of Education, School of Urban Construction and Environmental Engineering, Chongqing University, Chongqing 400044, China
[c] School of Environmental Science and Engineering, Sun Yat-sen University, Guangzhou 510275, China
[d] Guangdong Provincial Key Laboratory of Environmental Pollution Control and Remediation Technology, Sun Yat-sen University, Guangzhou 510275, China
[e] School of Environmental Science and Engineering, Suzhou University of Science and Technology, Suzhou 215009, China

ARTICLE INFO

Article history:
Received 22 April 2022
Revised 19 June 2022
Accepted 6 July 2022
Available online 8 July 2022

Keywords:
α-MnO_2 nanowires
Formation mechanism
Free-standing membrane
Fenton-like system

ABSTRACT

Assembling MnO_2 nanowires into macroscopic membrane is a promising engineered technology for catalyst separation and enhancement of Fenton-like reaction activity, yet its development is limited by the deficiencies in preparation and property modulation of the MnO_2 nanowires. In this work, we developed a facile method using C_2H_5OH and CH_3COOK as reductive and vital control reagents to react with $KMnO_4$ by hydrothermal reaction at 140 °C for 12 h, to prepare the ultralong α-MnO_2 nanowires up to tens of micrometers with high purity and aspect ratio. Such strategy not only had the advantages of being mild, easily controlled and environmental pollution-free, but also endowed α-MnO_2 nanowires with excellent ability as a Fenton catalyst when assembled into free-standing membrane for degrading phenolic compounds ($k_{obs} = 0.0738 \sim 0.1695$ min^{-1}) in a continuous flow reaction. The reactive oxygen species (*i.e.*, $^{\bullet}OH$) from Fenton-like reaction were enriched within this α-MnO_2 nanowire membrane *via* nanoconfinement effect, which further enhanced the mass transportation of $^{\bullet}OH$ available for phenolic contaminants. MnO_2 nanowire membrane using our method possessed the high practical potential for water purify due to its easy-preparation and enhanced catalytic performances.

Fenton-like advanced oxidation processes (AOPs) have been receiving lots of attentions in the fields of water treatment due to their low cost and high oxidation potentials [1–4]. Metal oxides exhibited high reactivities towards the catalyzed H_2O_2 propagations, which initiated radical chain reactions for pollutant degradation [5]. Manganese dioxide (MnO_2) was an efficient heterogenous catalyst to activate such processes, activating H_2O_2 to produce large amounts of superoxide anions ($O_2^{\bullet-}$) and hydroxyl radicals ($^{\bullet}OH$) [6,7]. Moreover, this catalyzed reaction would be promoted when framing MnO_2 to a nanosized shape with different crystal forms and facet exposures [8]. However, it was not practical to recycle and separate the suspended MnO_2 nanomaterials, thus limiting large-scale applications [9]. Some techniques of solving this issue have been developed, such as magnetic modification [10], support loading [11], and membrane construction [12]. Among these, assembling nanomaterials into macroscopic membrane was considered as the most promising engineered technology. The catalytic membrane not only promoted the potential of nanostructured MnO_2 separation and recovery, but also enhanced the Fenton-like reaction activity by confining such process in a nanodomain membrane pore [13,14]. The simultaneous filtration and reaction in confined space overcame the mass transfer limitations which often encountered in bulk diffusive mode operations [15,16]. Therefore, exploring facile approaches to prepare catalytic membrane using MnO_2 nanomaterials was urgent for practical applications.

Nanomaterials, enabling to be assembled into membrane, should be designed with special architectures to guarantee mechanical strength during the membrane filtration [17]. Assembling one dimensional (1D) MnO_2 nanowire into two-dimensional (2D) membrane by vacuum filtration was extensively used due to its advantages including easy-operation and liable controllability [18].

* Corresponding author.
** Corresponding author at: School of Environmental Science and Engineering, Sun Yat-sen University, Guangzhou 510275, China.
E-mail addresses: sunhit@hit.edu.cn (Z. Sun), zhushsh6@mail.sysu.edu.cn (S. Zhu).

https://doi.org/10.1016/j.cclet.2022.07.007
1001-8417/

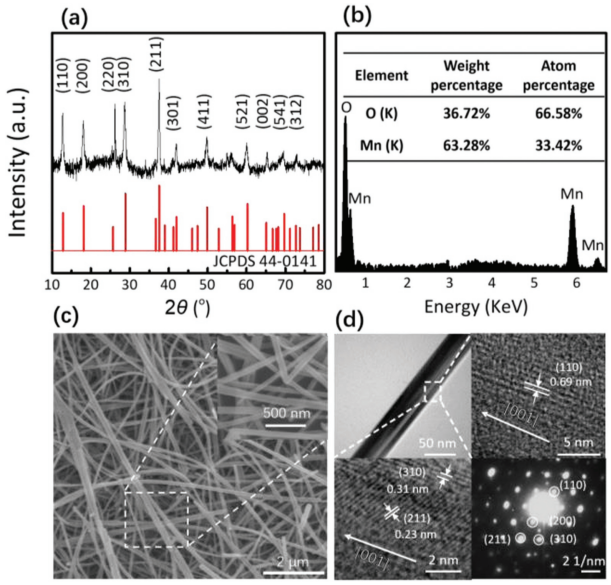

Fig. 1. (a) XRD pattern, (b) EDS spectrum, (c) SEM images and (d) HR-TEM images and SAED pattern of prepared MnO_2 nanowires.

In that case, it was prerequisite to prepare the well-structured MnO_2 nanowires. Some previous studies employed hydrothermal methods to accelerate the redox reactions of Mn hydrated ions by adding oxidative reagents (*e.g.*, HNO_3 or $(NH_4)_2S_2O_8$) to obtain MnO_2 nanowires [12,19,20]. However, for these current approaches, the reactions always concluded various extra components (mixed crystal) and byproducts (*e.g.,* MnOOH) [21]. Such issues would not only affect the purity of obtained MnO_2 nanowires, but also raised the difficulty of reaction control. In addition, since the vacuum filtration method required very high aspect ratio and good dispersion of MnO_2 nanowires in the solvents, few approaches could be applied in preparing such featured MnO_2 nanowires [12]. Therefore, studies on facile synthetic methods to obtain MnO_2 nanowires for catalytic membrane assembling and practical applications of water treatment were in great demands.

Herein, we developed a facile method to prepare ultralong α-MnO_2 nanowires with high purity and aspect ratio under 140 °C for 12 h through hydrothermal reaction. Specially, the C_2H_5OH and CH_3COOK were used as reductive and control reagents respectively to react with $KMnO_4$ as manganese source. Compared to previous studies [12,19,20], this strategy exhibited three advantages as follows: (1) This synthesis reaction was mild, easily controlled, and insensitive to temperature, reagents ratio, and reaction time; (2) the byproducts in reaction system were less and safer than those in other methods; (3) all reaction reagents were cheap, readily available, and environmentally friendly. We further investigated the formation mechanism of α-MnO_2 nanowires *via* various characterizations. Moreover, we assembled these α-MnO_2 nanowires into free-standing membrane as a Fenton catalyst for organic degradation in water. By the comparison with α-MnO_2 nanowire powder in aqueous solution, the possible mechanism of enhanced pollution removals and the application potential of α-MnO_2 nanowire membrane in Fenton-like oxidation were comprehensively explored.

Details of experimental procedures and characterizations were exhibited in Texts S1–S4 (Supporting information). The phase purity and crystal structure of the prepared MnO_2 were examined by XRD in Fig. 1a. All the diffraction peaks could be exclusively indexed as tetragonal α-MnO_2 (JCPDS No. 44-0141, space group I4/m, $a=b=9.784$ Å, $c=2.863$ Å), which was a type of the well-defined 2×2 tunnel structure with a tunnel size of 4.6 Å and was composed of edge shared MnO_6 octahedra with corner sharing double chains. No other characteristic peaks of the impurities were detected in the spectrum, indicating high phase purity of the obtained α-MnO_2 [20]. The elemental composition of α-MnO_2 was detected by EDS mapping (Fig. 1b). The atomic ratio of Mn to O was very close to 2, confirming that the highly purified α-MnO_2 was successfully synthesized. The morphology of α-MnO_2 was characterized by SEM and TEM. As shown in Fig. 1c, the α-MnO_2 were homogenously overlapped in a 1D nanowire shape as expected. The nanowire morphology grew into as long as tens of micrometers with diameter of ~50 nm (Fig. S1 in Supporting information). Such ultralong nanowires were ensured to form a stable membrane with high porosity and flexibility by easily interconnecting with each other [22]. Notably, a little number of bundles made up of ultralong nanowires (inset in Fig. 1c) parallelly coexisted with together, which indicated some details of "nucleation-growth" mechanism [21]. The ultralong nanowires were typical mesoporous structure (type II isotherm, Fig. S2 in Supporting information) and the BET surface area was up to 34.2 m^2/g, which would endow the as-prepared α-MnO_2 with excellent catalytic performance [23]. With the help of HR-TEM, the deeper microstructure of α-MnO_2 nanowires was investigated (Fig. 1d). The clear crystal lattices signified that the ultralong nanowire was single-crystalline with crystal orientation along [001] direction (*c* axis). Along the growth axis, the interplanar spacing was 0.69 nm, corresponding to the (110) facets. Two other interplanar spacings between the adjacent lattice planes were also measured to be 0.31 and 0.23 nm, which could be assigned to the (310) and (211) facets of α-MnO_2. Moreover, the SAED pattern displayed orderly spot arrays which were indexed to the (110), (200), (310) and (211) planes. Comparing the intensities of XRD diffraction peaks, it could be found that the intensities corresponding to exposed facets in α-MnO_2 were relatively stronger. As known, the exposed facets had high percentage of unsaturated atoms and great potential to react with low percentage of unsaturated atoms [24,25]. In addition, the high-index exposed facets were usually composed of high density of under-coordinated atoms, such as steps, edges, and kinks, serving as active sites. The successful synthesis of α-MnO_2 with high-index exposed facets would contribute to enhancing the catalytic activity [20].

The formation mechanism of α-MnO_2 nanowires was systematically discussed and proposed. C_2H_5OH and CH_3COOK were identified as the key factors in the formation of ultralong nanowire shaped α-MnO_2. C_2H_5OH acted as a mild reducing agent to react with manganese source, MnO_4^-. Redox potential of MnO_4^-/MnO_2 (0.588 V in neutral condition) was only slightly higher than that of CH_3COOH/C_2H_5OH (0.31 V in neutral condition) which acted as the reductive electrode couple (Eq. 1) [26]. Such approximately standard electrode potentials made the reaction mild and slow, facilitating the "nucleation-growth" process [12,27]. However, the reactive solution containing C_2H_5OH and MnO_4^- could only form flower shaped α-MnO_2 instead of nanowire shaped (Fig. 2a). The lateral growth of α-MnO_2 needed to be restricted to form nanowires. As seen in Eq. 1, the reaction between C_2H_5OH and MnO_4^- did not generate steric reagent, which led to lateral growth into the flower shape of obtained MnO_2.

$$4MnO_4^- + 3C_2H_5OH \rightarrow 4MnO_2 + 3CH_3COO^- + OH^- + 4H_2O \quad (1)$$

$$2MnO_4^- + 3CH_3CHO \rightarrow CH_3COOH + 2CH_3COO^- + 2MnO_2 + H_2O \quad (2)$$

$$4MnO_4^- + 3C_2H_5OH + 4H^+ \rightarrow 3CH_3COOH + 4MnO_2 + 5H_2O \quad (3)$$

$$CH_3COO^- + H_2O \rightarrow CH_3COOH + OH^- \quad (4)$$

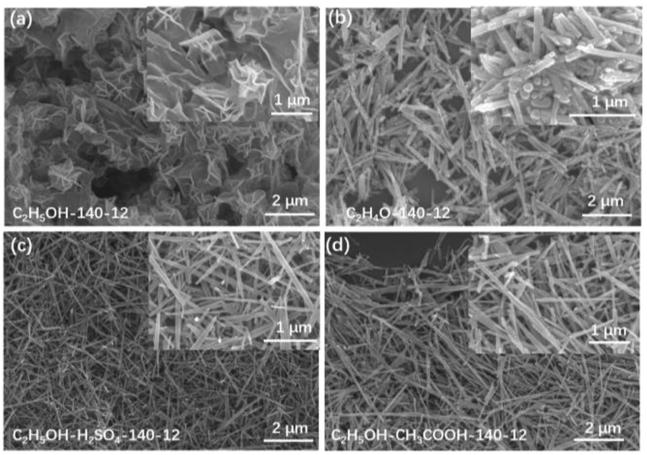

Fig. 2. SEM images of MnO_2 nanowires prepared under different conditions: (a) CH_3CH_2OH as reductive reagent at 140 °C for 12 h, (b) CH_3CHO as reductive reagent at 140 °C for 12 h, (c) CH_3CH_2OH as reductive reagent and H_2SO_4 as control reagent at 140 °C for 12 h, (d) CH_3CH_2OH as reductive reagent and CH_3COOH as control reagent at 140 °C for 12 h.

Previous study suggested that CH_3COOH could hinder the growth of lateral nanostructure through steric effects due to the formation of hydrogen bonds with -OH groups on MnO_2 [28]. For example, when employing CH_3CHO as a substitute of C_2H_5OH to reduce MnO_4^-, the formed MnO_2 transferred from flower-shape to nanowire-shape (Fig. 2b) due to the formation of byproduct CH_3COOH (Eq. 2). Moreover, both adding H^+ (*i.e.*, H_2SO_4) which enhanced the hydrolysis of generated CH_3COO^- to be CH_3COOH and directly adding CH_3COOH in C_2H_5OH/MnO_4^- system (Eq. 3) could further lead to the nanowire-shaped growth of MnO_2 (Figs. 2c and d). However, in the conditions outlined above, the obtained MnO_2 nanowires were short and seriously bonded with each other (Figs. 2b–d). This was because the gap of redox potential between electrode couple (*e.g.*, CH_3COOH/CH_3CHO (−0.12 V) < C_2H_5OH/CH_3COOH (0.31 V) in the neutral condition, MnO_4^-/MnO_2 (0.588 V in neutral condition) < MnO_4^-/MnO_2 (1.510 V in acidic condition)) in the reactive system became larger under these conditions, resulting in rapid formation of MnO_2 nuclei [29]. Too many nuclei of MnO_2 lowered the development of ultralong dendritic structure and further restricted the nanowire-shaped growth of MnO_2. To create a mild redox condition, CH_3COOK, which was also the only byproduct in the reaction system, was introduced into the reactive solution and the ultralong α-MnO_2 nanowires were obtained (Fig. 1c and Fig. S1). On the one hand, the hydrolysis of CH_3COO^- could generate CH_3COOH at the beginning of this reaction (Eq. 4). On the other hand, such process could produce extra OH^- which further decreased the gap of redox potential between CH_3COOH/CH_3CH_2OH and MnO_4^-/MnO_2 (0.564 V in base condition). This method created both steric configuration and mild reactive condition for well control of the ultralong growth of α-MnO_2 nanowires, and was insensitive to temperature, reagent ratio, and reaction time (Fig. S3 in Supporting information).

The formation mechanism of ultralong α-MnO_2 nanowires using our method was depicted in Fig. 3. Firstly, the primary nucleation of MnO_2 occurred slowly in the solution through the reaction between MnO_4^- and C_2H_5OH in weak base condition and formed three-dimension MnO_2 cores under hydrothermal condition. Then the hydrolysis of CH_3COOK leaded to the production of CH_3COOH attached to the surface of MnO_2 nuclei. When such reaction proceeded in a mild manner under steric effect of CH_3COOH, the MnO_2 intermediates grew along the c axis and formed ultralong nanowires slowly and homogenously. This approach was not only environmentally friendly and easily implemented, but also

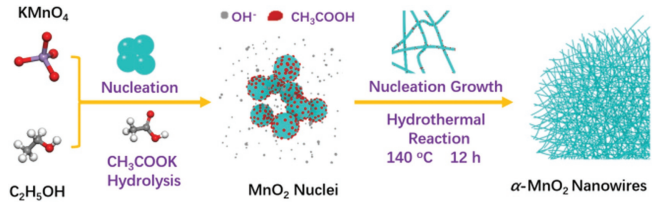

Fig. 3. Schematic illustration for the formation mechanism of α-MnO_2 nanowires.

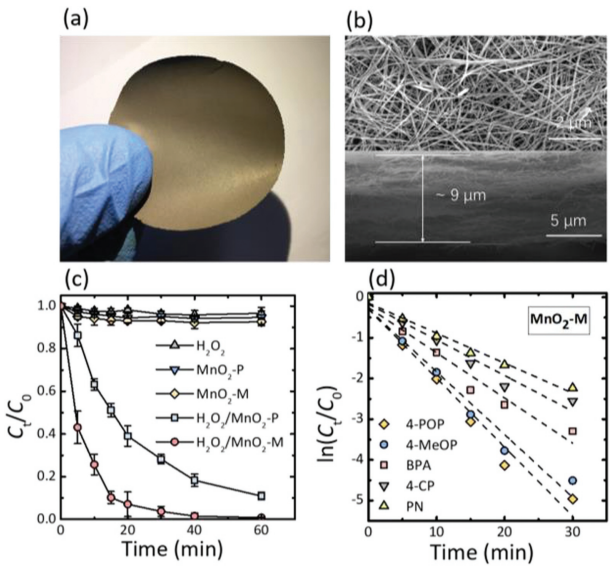

Fig. 4. (a, b) Digital photo and SEM images of obtained MnO_2 membrane, (c) BPA removal efficiency and (d) reactive rate constant for organic pollutants of MnO_2 membrane catalyzed H_2O_2 system. Condition: solution volume, 50 mL; MnO_2-M/MnO_2-P, 1 mg; H_2O_2, 50 mg/L; BPA, 2 mg/L; pH, 6.75; for continuous flow reaction (MnO_2-M), recycle solution speed, 50 mL/min; for batch reaction, stirring speed, 300 r/min.

forward-looking for developing other ultralong 1D nanostructures of metal oxides.

MnO_2 can enable Fenton-like chemistry and activate hydrogen peroxide (H_2O_2) to produce hydroxyl radicals (•OH) for organic pollutant degradation [5]. The catalytic performance of catalysts is intensively related to their application forms [30]. Herein, the catalytic performance of the relevant free-standing α-MnO_2 membrane (Figs. 4a and b) assembled by ultralong α-MnO_2 nanowires towards BPA degradation was deeply investigated. To exhibit the advantage of membrane catalyzation with continuous flow through MnO_2 membrane (MnO_2-M, Fig. S4 in Supporting information) over traditional heterogeneous catalytic process with bulk MnO_2 particle suspension (MnO_2-P, Fig. S4), systemically comparison of the removal process was conducted between MnO_2-M and MnO_2-P towards BPA. As shown in Fig. 4c, the removal of BPA by MnO_2-M, MnO_2-P, or H_2O_2 solution alone within 60 min was negligible (less than 10%) due to respective limited reactivity. When MnO_2 was coupled with H_2O_2, BPA removal was enhanced significantly because Fenton-like reaction was initiated and a large amount of •OH were generated to oxidize the aqueous organic contaminants. Particularly, the reactivity of MnO_2-M ($k_{obs} = 0.1112$ min^{-1}) confined within nanowire membrane was obviously higher than that of MnO_2-P ($k_{obs} = 0.0441$ min^{-1}) in bulk solution (Fig. 4c). Moreover, the catalytic reactivity of MnO_2-M was considerable for most of the model phenolic pollutants (Fig. 4d), in addition of the limited Mn^{2+} release less than 0.05 mg/L in reactive solution (Fig. S6 in Supporting information), indicating a preferable potential in practical application.

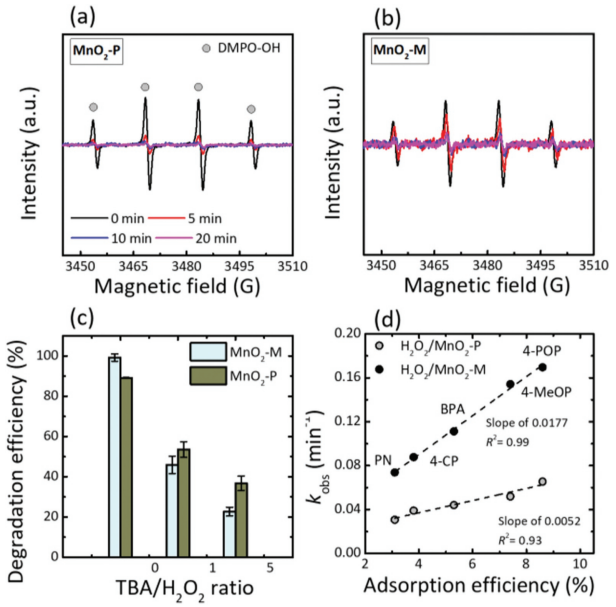

Fig. 5. (a, b) EPR spectrum at different reaction time of MnO_2 particle and MnO_2 membrane catalyzed H_2O_2 system, (c) variances of radical quenching tests under different TBA/H_2O_2 ratio, (d) relationship between adsorption capacity and reactive rate constant for several organic pollutants.

Due to the numerous channels or pores in membrane structure, the nanoconfinement effect is often hypothesized as a crucial factor for tuning membrane performance [30]. Therefore, it is speculated that the nanoconfinement effect could interpret this excellent performance when numerous channels (Fig. 4b) were observed to be developed within the ultralong α-MnO_2 nanowire membrane. Previous studies demonstrated that when chemical reactions occurred within a small or nanoscale confined space, their activity would be improved by altering the dielectric constant of water molecules, enrichment and exitance of reactants, or energy barriers [13,14,29,31]. Based on the second-order rate of BPA with $^{\bullet}OH$ (k_2 of 6.9×10^9 L mol^{-1} s^{-1}) [32], the steady-state $^{\bullet}OH$ concentration in MnO_2-M/H_2O_2 system (0.267 pmol/L) was approximately 2.5-fold higher than that in MnO_2-P/H_2O_2 system (0.107 pmol/L) [33]. This result indicated that more $^{\bullet}OH$ were exposed within the MnO_2-M to attack organic substrates due to the occurring nanoconfinement effect. When the overlapped α-MnO_2 nanowires created abundant channels or pores, the mass transfer of $^{\bullet}OH$ was confined and its exposed concentration became higher as the distance towards pore walls became smaller. The heterogeneous spatial distribution of $^{\bullet}OH$ avoided the long-ranged diffusion of short-lived free radicals and promoted the reaction kinetic rate within membrane compared to that on particles in bulk solution [14].

This proposal could be further identified by electron paramagnetic resonance (EPR) and quenching results. From the EPR results (Figs. 5a and b), it was observed that DMPO-OH intensity (Fig. 5b) changed slightly in MnO_2-M reactor within 60 min, when most of the confined $^{\bullet}OH$ near wall within the membrane were captured. However, the DMPO-OH intensity (Fig. 5a) decreased rapidly in MnO_2-P over time due to the fact that most surface generated $^{\bullet}OH$ were self-quenched in bulk solution (Eqs. 5 and 6) and were less available for DMPO scavenger.

$$^{\bullet}OH + H_2O_2 \rightarrow H_2O + HO_2^{\bullet} \quad (5)$$

$$^{\bullet}OH + {}^{\bullet}OH \rightarrow H_2O_2 \quad (6)$$

TBA was used as a quenching probe to evaluate the reactive efficiency of $^{\bullet}OH$ towards BPA in MnO_2-M and MnO_2-P [34]. Results showed that TBA exhibited higher quenching efficiency towards BPA removal in MnO_2-M/H_2O_2 system than in MnO_2-P/H_2O_2 system, regardless of TBA adding concentration (Fig. 5c). This phenomenon indicated that $^{\bullet}OH$ was more thermodynamically favorable to react with TBA in a confined interspace than in a bulk solution. The $^{\bullet}OH$ confined in the interspace of α-MnO_2 membrane was concentrated so that it possessed more collision probabilities with contaminants, resulting in enhanced efficiency during the reaction. As shown in Fig. 5d, the k_{obs} of different phenolic pollutants in both MnO_2-M/H_2O_2 (Fig. 4d) and MnO_2-P/H_2O_2 (Fig. S5 in Supporting information) systems were positively correlated with their adsorption efficiencies. Notably, slope of k_{obs} versus adsorption efficiency in MnO_2-M/H_2O_2 was higher than that in MnO_2-P/H_2O_2 system, indicating that the contaminant removal in MnO_2-M/H_2O_2 was more dependent on the reactions occurring around the surface possessing interface space. In a continuous flow reaction, the mass transportation between $^{\bullet}OH$ and phenolic compounds was confined in channels or pores, thus enhancing the oxidized kinetic rate [35].

In summary, our facile method for the preparation of ultralong α-MnO_2 nanowire membrane exhibited two following advantages. On the one hand, such easy and environmentally friendly method built a mild redox surrounding and steric hindrance to control the growth of α-MnO_2 nanowires. On the other hand, the α-MnO_2 membrane obtained by assembling these α-MnO_2 nanowires could create abundant channels or pores, triggering the nanoconfined effect to enrich the reactive oxygen species ($^{\bullet}OH$) available for targeted contaminants in Fenton-like reaction. This study not only established a novel method to prepare ultralong α-MnO_2 nanowires, but also pointed out a potential application form of nanowire-shaped Fenton catalysts in environmental remediation.

Declaration of competing interest

The authors declare no conflict of interest.

Acknowledgments

The support from National Natural Science Foundation of China (Nos. 52000050, 52100024 and 42007115), Postdoctoral Science Foundation of China (Nos. 2019M663245 and 2020M670913), Heilongjiang Postdoctoral Fund (No. LBH-Z20063) and State Key Laboratory of Urban Water Resource and Environment (Harbin Institute of Technology) (Nos. 2021TS22 and QAK202111) are greatly appreciated.

Supplementary materials

Supplementary material associated with this article can be found, in the online version, at doi:10.1016/j.cclet.2022.07.007.

References

[1] K. Chen, G.H. Wang, W.B. Li, et al., Chin. Chem. Lett. 25 (2014) 1455–1460.
[2] Z. Shangguan, X. Yuan, L. Jiang, et al., Chin. Chem. Lett. 33 (2022) 4719–4731.
[3] Y. Liu, F. Liu, N. Ding, et al., Chin. Chem. Lett. 31 (2020) 2539–2548.
[4] Y. Liu, F. Li, Q. Xia, et al., Nanoscale 10 (2018) 4771–4778.
[5] Y. Zhang, C. Liu, B. Xu, F. Qi, W. Chu, Appl. Catal. B: Environ. 199 (2016) 447–457.
[6] Z. Wan, J. Wang, J. Hazard. Mater. 324 (2017) 653–664.
[7] E. Saputra, S. Muhammad, H. Sun, et al., Environ. Sci. Technol. 47 (2013) 5882–5887.
[8] S. Zhu, S.H. Ho, C. Jin, X. Duan, S. Wang, Environ. Sci. Nano 7 (2020) 368–396.

[9] Y. Liu, M. Tourbin, S. Lachaize, P. Guiraud, Powder Technol. 255 (2014) 149–156.
[10] J. Zhao, J. Liu, N. Li, et al., Chem. Eng. J. 304 (2016) 737–746.
[11] L. Zhao, J. Ma, Z.Z. Sun, X.D. Zhai, Appl. Catal. B: Environ. 83 (2008) 256–264.
[12] B. Lan, L. Yu, T. Lin, et al., ACS Appl. Mater. Interfaces 5 (2013) 7458–7464.
[13] J. Qian, X. Gao, B. Pan, Environ. Sci. Technol. 54 (2020) 8509–8526.
[14] S. Zhang, M. Sun, T. Hedtke, et al., Environ. Sci. Technol. 54 (2020) 10868–10875.
[15] J. Wang, H. Guo, Z. Yang, Y. Mei, C.Y. Tang, J. Membr. Sci. 525 (2017) 298–303.
[16] Y. Xie, Y. Liu, Y. Yao, et al., Chin. Chem. Lett. 33 (2022) 1298–1302.
[17] H. Jiang, T. Zhao, J. Ma, C. Yan, C. Li, Chem. Commun. 47 (2011) 1264–1266.
[18] J.W. Liu, H.W. Liang, S.H. Yu, Chem. Rev. 112 (2012) 4770–4799.
[19] F. Cheng, J. Zhao, W. Song, et al., Inorg. Chem. 45 (2006) 2038–2044.
[20] S. Rong, P. Zhang, F. Liu, Y. Yang, ACS Catal. 8 (2018) 3435–3446.
[21] X. Wang, Y. Li, J. Am. Chem. Soc. 124 (2002) 2880–2881.
[22] X. Wang, S. Ni, G. Zhou, et al., Mater. Lett. 64 (2010) 1496–1498.
[23] X. Wang, L. Dou, L. Yang, J. Yu, B. Ding, J. Hazard. Mater. 324 (2017) 203–212.
[24] S. Annabella, Nat. Mater. 7 (2008) 613.
[25] A. Vittadini, A. Selloni, F.P. Rotzinger, M. Grätzel, Phys. Rev. Lett. 81 (1998) 2954–2957.
[26] J. Bertsch, A.L. Siemund, F. Kremp, V. Muller, Environ. Microbiol. 18 (2016) 2913–2922.
[27] G. Cheng, S. Xie, B. Lan, et al., J. Mater. Chem. A 4 (2016) 16462–16468.
[28] Q. Zhang, X. Cheng, X. Feng, et al., J. Mater. Chem. 21 (2011) 462–465.
[29] J. Yuan, W.N. Li, S. Gomez, S.L. Suib, J. Am. Chem. Soc. 127 (2005) 14184–14185.
[30] Y. Chen, G. Zhang, H. Liu, J. Qu, Angew. Chem. Int. Ed. 58 (2019) 8134–8138.
[31] X. Ai, Y.H. Li, Y.W. Li, T. Gao, K.G. Zhou, Chin. Chem. Lett. 33 (2022) 2832–2844.
[32] J.R. Peller, S.P. Mezyk, W.J. Cooper, Res. Chem. Intermed. 35 (2009) 21–34.
[33] S. Zhang, T. Hedtke, Q. Zhu, et al., Environ. Sci. Technol. 55 (2021) 9266–9275.
[34] D. Yuan, C. Zhang, S. Tang, et al., Chin. Chem. Lett. 32 (2021) 3387–3392.
[35] Y. Oaki, H. Imai, Angew. Chem. 119 (2007) 5039–5043.